A new, improved and fully automatic method for teleseismic depth estimation of moderate earthquakes (4.5 < *M* < 5.5): application to the Guerrero subduction zone (Mexico)

Jean Letort,[1] Jocelyn Guilbert,[2] Fabrice Cotton,[3] István Bondár,[4] Yoann Cano[2] and Julien Vergoz[2]

[1]*CEA, DAM, DIF, F-91297 Arpajon, France & Isterre, Grenoble, France. E-mail: jean.letort@ujf-grenoble.fr*
[2]*CEA, DAM, DIF, F-91297 Arpajon, France*
[3]*GeoForschungsZentrum, Helmholtz Centre Potsdam, Potsdam, Germany*
[4]*ISC, Thatcham, England*

SUMMARY

The depth of an earthquake is difficult to estimate because of the trade-off between depth and origin time estimations, and because it can be biased by lateral Earth heterogeneities. To face this challenge, we have developed a new, blind and fully automatic teleseismic depth analysis. The results of this new method do not depend on epistemic uncertainties due to depth-phase picking and identification. The method consists of a modification of the cepstral analysis from Letort *et al.* and Bonner *et al.*, which aims to detect surface reflected (pP, sP) waves in a signal at teleseismic distances (30°–90°) through the study of the spectral holes in the shape of the signal spectrum. The ability of our automatic method to improve depth estimations is shown by relocation of the recent moderate seismicity of the Guerrero subduction area (Mexico). We have therefore estimated the depth of 152 events using teleseismic data from the IRIS stations and arrays. One advantage of this method is that it can be applied for single stations (from IRIS) as well as for classical arrays. In the Guerrero area, our new cepstral analysis efficiently clusters event locations and provides an improved view of the geometry of the subduction. Moreover, we have also validated our method through relocation of the same events using the new International Seismological Centre (ISC)-locator algorithm, as well as comparing our cepstral depths with the available Harvard–Centroid Moment Tensor (CMT) solutions and the three available ground thrust (GT5) events (where lateral localization is assumed to be well constrained with uncertainty <5 km) for this area. These comparisons indicate an overestimation of focal depths in the ISC catalogue for deeper parts of the subduction, and they show a systematic bias between the estimated cepstral depths and the ISC-locator depths. Using information from the CMT catalogue relating to the predominant focal mechanism for this area, this bias can be explained as a misidentification of sP phases by pP phases, which shows the greater interest for the use of this new automatic cepstral analysis, as it is less sensitive to phase identification.

Key words: Fourier analysis; Earthquake source observations; Seismic monitoring and test-ban treaty verification; Body waves.

INTRODUCTION

Trustworthy depth estimations of moderate earthquakes (4 < *M* < 5) are of great importance in seismology. The knowledge of earthquake depth distributions in exposed areas is crucial to evaluate scenarios for future damaging earthquakes. More generally, earthquake depths contribute to our interpretation of the Earth structure and to our understanding of tectonic processes; for example, by constraining subduction geometries. Depth estimations are also important for other applications, such as event screening (e.g. earthquake versus explosion) for compliance with the Comprehensive Nuclear Test Ban Treaty.

Unfortunately, in many cases, the depth of an earthquake is difficult to estimate. Bondár *et al.* (2004) showed that focal depths are poorly constrained by direct phases at almost all distance ranges (except for very short distances): the travel-time residuals are

relatively insensitive to depth changes of large events because of the trade-off between depth and origin time. If the absolute direct phase-arrival values have little impact on depth resolution, the delays between the arrival times of surface-reflected phases (pP, sP) and the direct P wave contain important useful information on the focal depth. Indeed, in a given velocity model (e.g. International Association of Seismology and Physics of the Earth Interior 1991 [IASPEI91]), these time delays between the downgoing waves (P waves) and the upgoing surface-reflected waves (pP or sP, eventually pwP, swP) provide good estimations of the source depths and have often been used to constrain depths in global catalogues (Engdahl *et al.* 1998; Bondár *et al.* 2004; Bondár & Storchak 2011). However, these phases are often difficult to detect with precision, as they are commonly convolved into one group of mixed phases (Bondár *et al.* 2004). Even when these depth phases are clear, they are often misidentified by analysts (e.g. pP instead of sP, or pwP, PcP). Hence, Engdahl *et al.* (1998) showed that re-identification of these phases is needed to improve focal depths.

To face these difficulties, we have developed a new, blind, and fully automatic teleseismic depth analysis that is independent of epistemic uncertainties due to phase picking and identification. The method is a modification of the cepstral analysis method from Letort *et al.* (2014), and it aims to detect these surface-reflected waves in a signal at teleseismic distances (pP and sP waves). The key point for the success of this method is our computation of the automatic detection of the depth phases in a signal, and their identification without any *a priori* and analyst-subjective judgment.

To test our new method, an interesting application was found in the Guerrero area (Mexico). In subduction contexts, studies of hypocentre locations (e.g. Pardo & Suarez 1995) provide an idea of subduction geometries, which are crucial to understand the different phenomena that have roles in these subductions, but which are usually limited by uncertainties in depth estimation. In the case of the Guerrero subduction, there is a burning open debate about the lateral variations of the subducted plate geometry, which might have a role in the 'slow silent earthquakes' that have been observed there, and which have great impact on the amount of accumulated slip along this subduction zone.

We thus conducted a detailed analysis of the Guerrero depth distribution based on the International Seismological Centre (ISC) catalogue, and tested our method in this specific case study. We estimated depths for 152 recent earthquakes (post-2002) with magnitudes >4.5. Twenty-two stations/arrays from the Incorporated Research Institutions for Seismology (IRIS) were selected for this study (between 28° and 90°). The stations are part of the Air Force Technical Applications Center and the IRIS networks (II, IU). Note that most of the selected stations are in North America, and that the azimuthal coverage shows a maximal gap (for the Pacific part) of 180°. The recordings were requested from the IRIS web service without any quality criteria, which makes our method completely blind and reproducible. However, according to the dates of the events, the operating dates of the different sensors, and the availability of the data through the IRIS website, we did not access the whole set of stations each time, and we generally obtained between 15 and 20 recordings for each event.

Finally, our new cepstral analysis was applied to each beam of the selected array and for each station. In the next section, our proposed new methodology is described, beginning with a description of previous common difficulties when using classical cepstral methods.

Limitations of classical cepstral analysis

The usual main assumption of any cepstral method is to consider a teleseismic signal $f(t)$ as a direct P wave $S(t-T_0)$, and with an echo, the pP reflected wave [$S(t-T_1)$]. This echo should have the same frequency content as the source (direct P waves), with only a delay $T_1 - T_0$ in time, as indicated in eq. (1):

$$f(t) = a_0 S(t - T_0) + a_1 S(t - T_1) \quad t > 0, \tag{1}$$

where t is the current sampling point, the signal $f(t)$ has a duration of $D = fe * N$ s, with N as the number of samplings for f. T_0, T_1 and $\in \mathbb{N}^*$ are the sampling positions for the two phase arrivals, fe is the sampling frequency (the arrival time for the P-phase (number 0) is $\frac{T_0}{fe}$ s).

From this assumption, and working in the spectral domain, the cepstral method automatically and efficiently detects the delay $T_1 - T_0$ between the two phases, through the study of the spectral modulation of the source from the echo, as shown, for instance, by Cohen (1970), Childers *et al.* (1977), Bonner *et al.* (2002) and Letort *et al.* (2014). Indeed, with ω as the pulsation, ($\omega = 2\pi f$, in the Fourier domain, this becomes as in eq. (2):

$$F(w) = \left(a_0 e^{-i\omega T_0} + a_1 e^{-i\omega T_1}\right) \frac{1}{N} \int_0^N S(t) e^{-i\omega t} dt. \tag{2}$$

The cepstrum of $f(t)$ is then given by eq. (3):

$$Cep_f(t) = \frac{1}{2\pi} \int_0^{2\pi} \ln|F(w)|^2 e^{i\omega t} dw. \tag{3}$$

Combining eqs (2) and (3), the analytical cepstrum of eq. (4) can be estimated:

$$Cep_f(t) = \frac{1}{2\pi} \int \ln(|1 + X|) e^{i\omega t} dw + Cep_S(t), \tag{4}$$

where $|X| = |A_{12} \cos(w(T_1 - T_0))| < 1$, $A_{12} = \frac{2a_0 a_1}{a_0^2 + a_1^2}$.

As $|X| < 1$, the logarithm $\ln(|1 + X|)$ in eq. (4) can be expanded in a power series and truncated to the order 1 (according to the theorem of alternating functions). This is one key assumption for the classical cepstrum analysis that allows the derivation of eq. (5): the power cepstrum has a peak linked to the delay between the P wave and pP, and the amplitude is $\frac{A_{12}}{2}$.

$$Cep_f(t) - Cep_S(t) = \frac{1}{2\pi} \int X e^{i\omega t} dw$$

$$= A_{12} \frac{1}{2\pi} \int \cos(w(T_1 - T_0) e^{i\omega t} dw$$

$$= \frac{A_{12}}{2} \delta(t - (T1 - T0)). \tag{5}$$

Hence, according to eq. (5), if we can correctly correct from the source term $Cep_S(t)$, in a simple case with a direct impulsive P wave and a single pP reflected wave, the cepstral analysis is very well suited and of great interest for estimation of the delay between the two phases, and then of the depth, using the relationship between the epicentral distance, the source depth, and the P–pP delay in the traveltime tables.

However, this classical cepstrum analysis is limited in more complex and realistic cases with different reflections for the P-coda (sP or P-S conversion, subduction interface reflection). For instance, one major limitation comes when the P wave has weak energetic content, and the P coda has two or more predominant phases, classically as pP and sP. In this case, the echo in the signal will be linked to the pP/sP delay, and not to the P/pP or P/sP delay. The
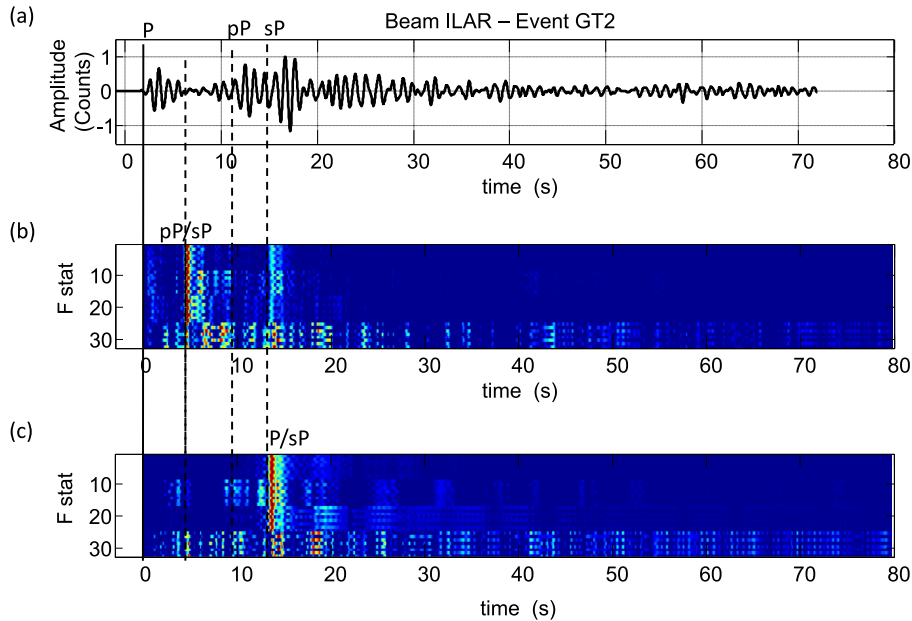
Figure 1. (a) Recording of the GT2 event in the Guerrero area, at 25 km in depth (Table 1), and where the localization is assumed to be well constrained. Three phases are detected: P, pP and sP. (b) Classical cepstrum analysis using eq. (5) and removing the main trend of the signal, following Letort *et al.* (2014). The main peak comes from the pP–sP delay and does not allow information on the depth to be deduced. (c) Cepstrum analysis for the new method, from eq. (8), with subtraction of the cepstrum due to the coda. The main peak in the cepstrum is well linked to the P–sP delay.

resulting depth estimation will be completely incorrect, as the depth depends on the delay between the downgoing phase (*P*-wave) and the upgoing waves (pP, sP), and not on the delays between only the upgoing waves that dominate the teleseismic signal here. A good illustration of this difficulty can be seen in Figs 1(a) and (b), where a weak *P* wave and clear strong pP and sP are not correctly detected by the cepstral analysis (for this reason it is generally assumed that the P–pP delay is among the three main peaks of the cepstrum).

Another important issue during cepstral analysis is to take into account the possible effects of the source term of the cepstrum *Cep_S*(*t*), as in eq. (5). For instance, Letort *et al.* (2014) removed the main trend of the spectrum as the *P*-wave contribution to the spectrum. However, in the case of a complex *P* wave, this trend might be an incorrect representation of the source spectrum, as smoother than predicted. We thus developed a new cepstral analysis, taking account of two echoes (or more) instead of a single echo, and with a new way of correcting the source effect.

New cepstral definition using three phase arrivals (two echoes)

To improve our ability to automatically take into account different depth phases and to have a trustworthy identification of these phases, we developed a new cepstral method that is based on the presence of two main echoes in a signal, instead of the common assumption of one single depth phase arrival. These echoes can preferentially be pP and sP phases, and as was shown by Pearce & Rogers (1989), a teleseismic signal is mainly dominated by the three phase arrivals of *P* waves, pP and sP. This can also be extended, for instance, to pP and PcP phase detection, or other converted/reflected phases that are not linked to the free surface (e.g. converted/reflected waves in the subduction interface). For this new proposed method, our assumptions here are that:

(1) It is possible to isolate in time the direct *P* waves from the later part of the coda.

(2) The P coda is dominated by at least one reflection due to the free surface (pP and/or sP).

(3) The P coda contains information about the source, so it is composed of the depth phases and/or of other different echoes (e.g. PcP, pwP, pmP and so on) and/or some reflected or converted waves that have the same frequency content as the direct P source.

(4) The source term *S*(*t*) is a short arrival of less than 2–3 s. The depth phases are thus well separated in time from the direct *P* wave (this assumption is needed only to take advantage of the signal power; see next sections).

Under these assumptions, the cepstral methodology can be rewritten for two echoes, for instance, in the typical case where a signal is characterized by a *P* wave and by two depth phases (pP and sP):

$$f(t) = a_0 S(t - T_0) + a_1 S(t - T_1) + a_2 S(t - T_2), \quad t > 0, \quad (6)$$

where *t* is the current sampling point, and $T_0, T_1, T_2 \in \mathbb{N}^*$. We assume that *S*(*t*) is null everywhere except for the time of the direct *P*-wave arrival, the source arrival, so for a few seconds (a maximum of 3 s). Hence $S(t) = 0$, except for $t < fe * 3$ (where *fe* is the frequency sampling). In the Fourier domain, this gives eq. (7):

$$F(w) = \left(a_0 e^{-i\omega T_0} + a_1 e^{-i\omega T_1} + a_2 e^{-i\omega T_2}\right) \frac{1}{N} \int_N^1 S(t) e^{-i\omega t} dt. \quad (7)$$

Combining eqs (3) and (7), it is possible to estimate the analytical cepstrum of eq. (8):

$$Cep_f(t) = \frac{1}{2\pi} \int \ln(|1 + A_{12}\cos(w(T_1 - T_0)) $$
$$+ A_{13}\cos(w(T_2 - T_0)) + A_{23}\cos(w(T_2 - T_1))|) $$
$$\times e^{i\omega t} dw + Cep_S(t), \quad (8)$$

where $A_{12} = \frac{2a_0 a_1}{a_0^2 + a_1^2 + a_2^2}$, $A_{13} = \frac{2a_0 a_2}{a_0^2 + a_1^2 + a_2^2}$, $A_{23} = \frac{2a_1 a_2}{a_0^2 + a_1^2 + a_2^2}$, and where *Cep_S*(*t*) is the cepstrum due to the source *S*(*t*), the direct *P* wave.
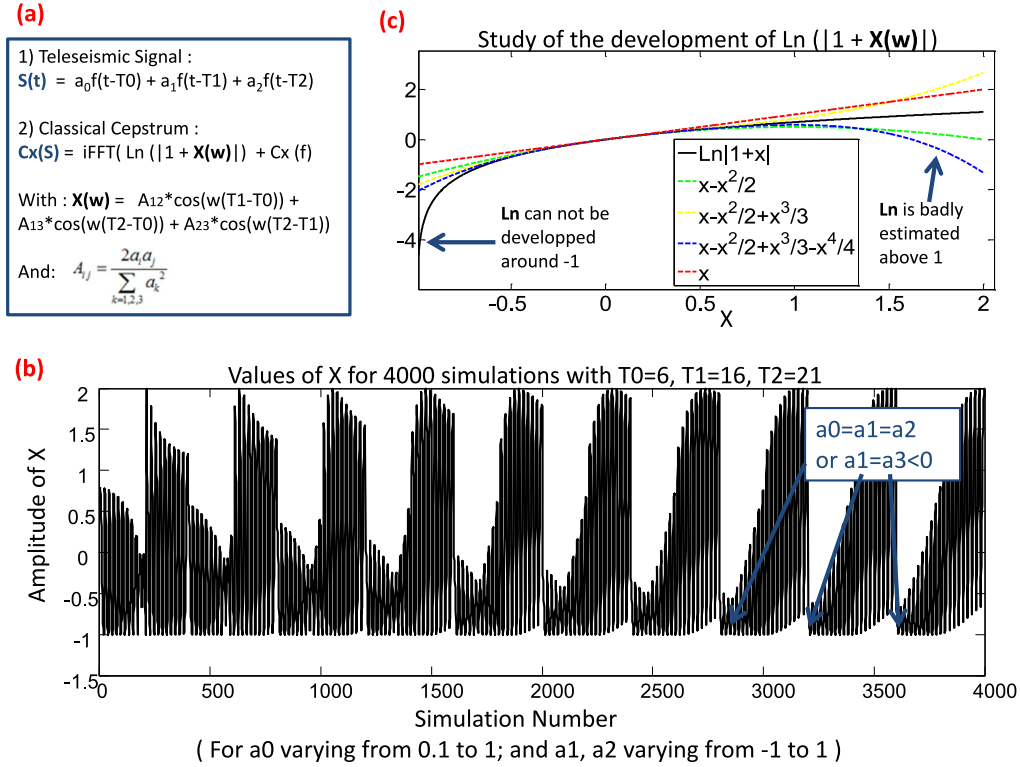
(a)

1) Teleseismic Signal :
$S(t) = a_0 f(t-T0) + a_1 f(t-T1) + a_2 f(t-T2)$

2) Classical Cepstrum :
$Cx(S) = iFFT(Ln (|1 + X(w)|) + Cx (f)$

With : $X(w) = A_{12}*\cos(w(T1-T0)) + A_{13}*\cos(w(T2-T0)) + A_{23}*\cos(w(T2-T1))$

And: $A_{ij} = \dfrac{2a_i a_j}{\sum\limits_{k=1,2,3} a_k^2}$

(c)

Study of the development of Ln (|1 + **X(w)**|)

Ln|1+x|
$x-x^2/2$
$x-x^2/2+x^3/3$
$x-x^2/2+x^3/3-x^4/4$
x

Ln can not be developped around -1

Ln is badly estimated above 1

X

(b)

Values of X for 4000 simulations with T0=6, T1=16, T2=21

a0=a1=a2 or a1=a3<0

Amplitude of X

Simulation Number

(For a0 varying from 0.1 to 1; and a1, a2 varying from -1 to 1)

Figure 2. (a) Expansion in the power series of ln(|1 + X|) according to the different possible values of X. The four first orders are plotted. At around −1, the logarithm tends to −∞. Above 1.5, the difference between the logarithm and the power series becomes important. (b) Values of X from eq. (10), for 4000 simulations computed by making a_0 vary from 0.1 to 1 by 0.1, a_1 and a_2 from −1 to 1 by 0.1, and ω from 2pi/100 to 2pi by 2pi/100. T_0, T_1 and T_2 are fixed at 6, 16 and 21 s. It can be seen that X varies between −1 and 2. The values −1 are reached when $a_0 = a_1 = a_2$ or when $a_1 = a_2 < 0$. For other values of T_0, T_1, T_2, X is always between −1 and 2.

Hence, this gives eq. (9):

$$Cep_f(t) = \frac{1}{2\pi} \int \ln(|1 + X(w)|)\, e^{i\omega t}\, dw + Cep_S(t) \qquad (9)$$

with

$$|X(w)| = |A_{12} \cos(w(T_1 - T_0)) + A_{13} \cos(w(T_2 - T_0)) + A_{23} \cos(w(T_2 - T_1))|. \qquad (10)$$

Hence, in the case of three phase arrivals, $X(\omega)$ reaches values between −1 and 2, according to the combination of T_0, T_1, T_2, a_0, a_1, a_2 and ω (Fig. 2). $X(w)$ is mainly between −0.7 and 1.5 (Fig. 2b), where the approximation of the logarithm by the expansion of the power series appears acceptable (see Fig. 2a). Under this approximation, using classical trigonometry relations, eq. (6) can be written as the inverse transform of a summation of a combination of cosines. Hence, the cepstrum is zero everywhere except for punctual delays, where a Dirac is observed, which is equivalent to a peak in the cepstrum (by the definition of the inverse transform).

In eq. (11), we show the expansion of the cepstrum to the order 1:

$$Cep_f(t) - Cep_S(t) = \frac{1}{2\pi} \int X\, e^{i\omega t}\, dw$$
$$= \frac{A_{12}}{2} \delta(t - (T1 - T0))$$
$$+ \frac{A_{13}}{2} \delta(t - (T2 - T0))$$
$$+ \frac{A_{23}}{2} \delta(t - (T2 - T1)). \qquad (11)$$

In eq. (11), there is an important peak for the delay $T_2 - T_1$ (sP/pP), as shown in Fig. 1 and in the theoretical example in Fig. 3(b).

Eq. (11) is often an acceptable representation of the cepstrum peaks and amplitudes, and we then decided to use this new theoretical definition of the cepstrum, based on three arrivals. However, the expansion of the logarithm is not valid for a few points. In particular, when $a_0 = a_1 = a_2$ or when $a_0 > 0$ and $a_1 = a_2 < 0$, X can reach −1 (Fig. 2b), which makes the value of the logarithm equal to infinity, and the cepstrum is then divergent. Hence, the exact cepstrum function cannot be always estimated from eq. (11).

To investigate these singular points more deeply, and to test our new cepstrum definition, we studied statistically the possible peaks for the cepstrum, with the testing of different values of amplitudes and delays for the three phase arrivals. Thus, we defined a signal with a first P-phase with its amplitude varying between 0.1 and 1, every 0.1; followed by the pP and sP phases with amplitudes varying between −1 and 1, every 0.1. Fig. 3 shows an example of our investigations, for fixed P wave, pP and sP arrival times. In a few cases where $a_2 = a_3 < 0$, the inverse Fourier transform is divergent and the cepstra show no peaks. For more than 90 per cent of the simulations, the maxima of the cepstra are well linked to one of the three delays (P–pP, P–sP, sP–pP), which validates the relation proposed in eq. (11) for these cases. In Fig. 3(b), almost 25 per cent of the simulated cepstra have their maximum related to the delay sP–pP, which is not what is needed for correct depth estimation.

To remove this effect of the sP–pP echo, we wished to compute another cepstrum, only on the coda part of the signal (removing the P phase). This will allow the echo(es) due to the later phases that interact together to be identified, and to be removed.
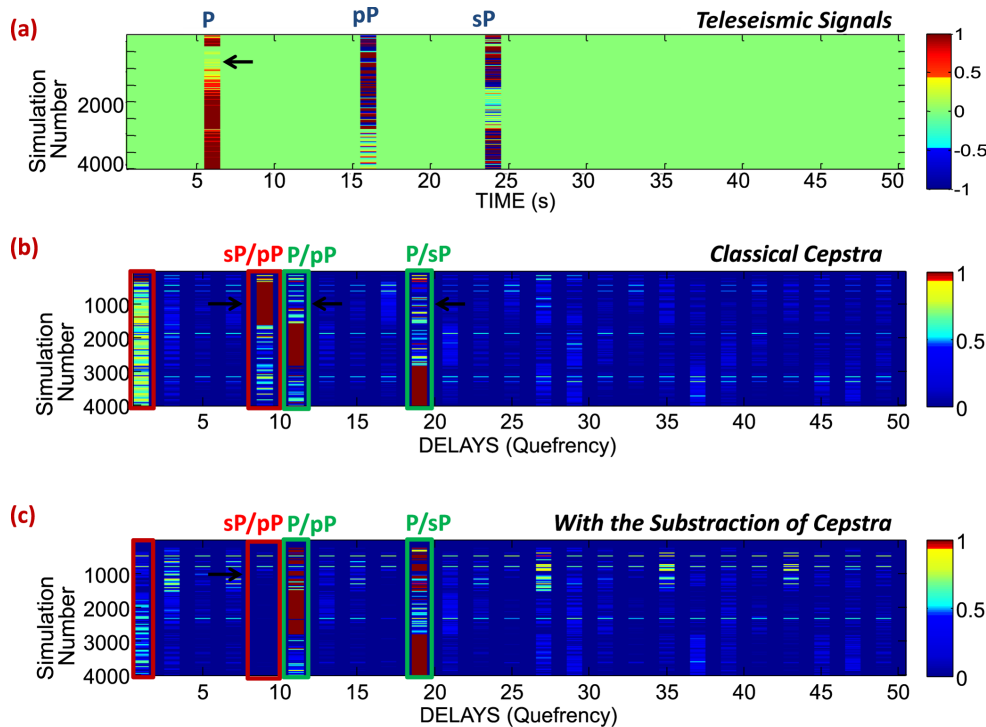
Figure 3. (a) Different simulations of recordings with different amplitudes a_0, a_1, a_2. (b) Associated numerical cepstra computed using the inverse Fourier transform of $\ln(|1 + X|)$ (see eq. 9). We assumed that the source was perfectly removed in the spectrum domain. Note that some simulations show no peaks, or maxima for the first points of the cepstra, where $a_0 = a_1 = a_2 > 0$ or $a_1 = a_2 < 0$. Note that the main delays of P–pP, P–sP are well found, as well as the not needed sP–pP delay. This delay is predominant in the cepstra when a1 is small and when $|a_0|$, $|a_1|$ are large, for almost 1000 simulations (among 4000 in total). (c) Numerical cepstra for the new cepstral method proposed in eq. (14b). Note that the peaks related to the pP/sP delays have been removed and the divergence for each of the first points of the cepstra have decreased.

Removing the pP/sP echo

We can thus proceed to the same development with the P coda part only, with the removal of the direct P wave $S(t)$:

$$g(t) = a_1 S(t - T_1) + a_2 S(t - T_2). \tag{12}$$

With only two phases, the development in the power series to the order 1 is possible (eq. 5), and the cepstrum can be written as in eq. (13):

$$Cep_g(t) - Cep_S(t) = \frac{B_{23}}{2} \delta(t - (T2 - T1)), \tag{13}$$

where $B_{23} = \frac{2a_1 a_2}{a_1^2 + a_2^2}$. In eq. (13), all of the terms are zeroes except for $t = (T_2 - T_1)$.

Finally, combining eqs (11) and (13), we can define our final cepstral method, as seen by eq. (14a):

$$CEP\_FINAL(t) = |Cep_f(t) - Cep_g(t)| \tag{14a}$$

with,

$$Cep_f(t) - Cep_g(t) = Cep_S(t) - Cep_S(t) + \frac{A_{12}}{2}\delta(t - (T1 - T0))$$

$$+ \frac{A_{13}}{2}\delta(t - (T2 - T0)) + \left(\frac{A_{23}}{2} - \frac{B_{23}}{2}\right)$$

$$\times \delta(t - (T2 - T1)). \tag{14b}$$

Using eq. (14b), two major improvements to the classical cepstral analysis have been made. First, the source term $Cep_S(t)$ has been removed automatically, with the only *a priori* assumption being that the later phases contain information about the source, which is a reasonable assumption, and especially in the case of subduction

environments where the P coda is usually long and shows numerous reflections/conversions due to the complexity of the source medium. Above all, the great new advantage of this method is that in the analytical eq. (14b) of the cepstrum, we have reduced the effects of the echoes that are not directly due to the direct P waves, but only because of the delayed interference between the pP and sP phases. We have also investigated statistically the efficiency of this proposed method, as shown in Fig. 4: using the subtraction of the cepstra, 86 per cent of the simulated cepstra have their maxima linked to the P–pP or P–sP delay, while the classical ceptrum has only 62 per cent success.

This result can be extended in cases of a signal with >2 echoes. All of the peaks in the cepstrum that are due to later phases that interfere with each other are reduced, which is of great interest for cesptrum peak interpretation. In Fig. 1, the result of the cepstrum analysis using the classical method has been plotted (Fig. 1b) for a real event in the Guerrero area, at 25 km in depth (Table 1): the main peak in the cepstrum comes from the pP–sP delay and does not allow information on depth to be deduced. On the contrary, for the new method (Fig. 1c), with the subtraction of the cepstrum due to the coda, the main peak in the cepstrum is well linked to the P–sP delay.

Focusing on the predominant reflection in the cepstrum analysis using the power of the teleseismic signal

Taking the power of the signal, if we assume that the phases are distinct, we obtain eq. (15) as:

$$f^n(t) = a_0^n S^n(t - T_0) + a_1^n S^n(t - T_1) + a_2^n S^n(t - T_2), \quad t > 0. \tag{15}$$
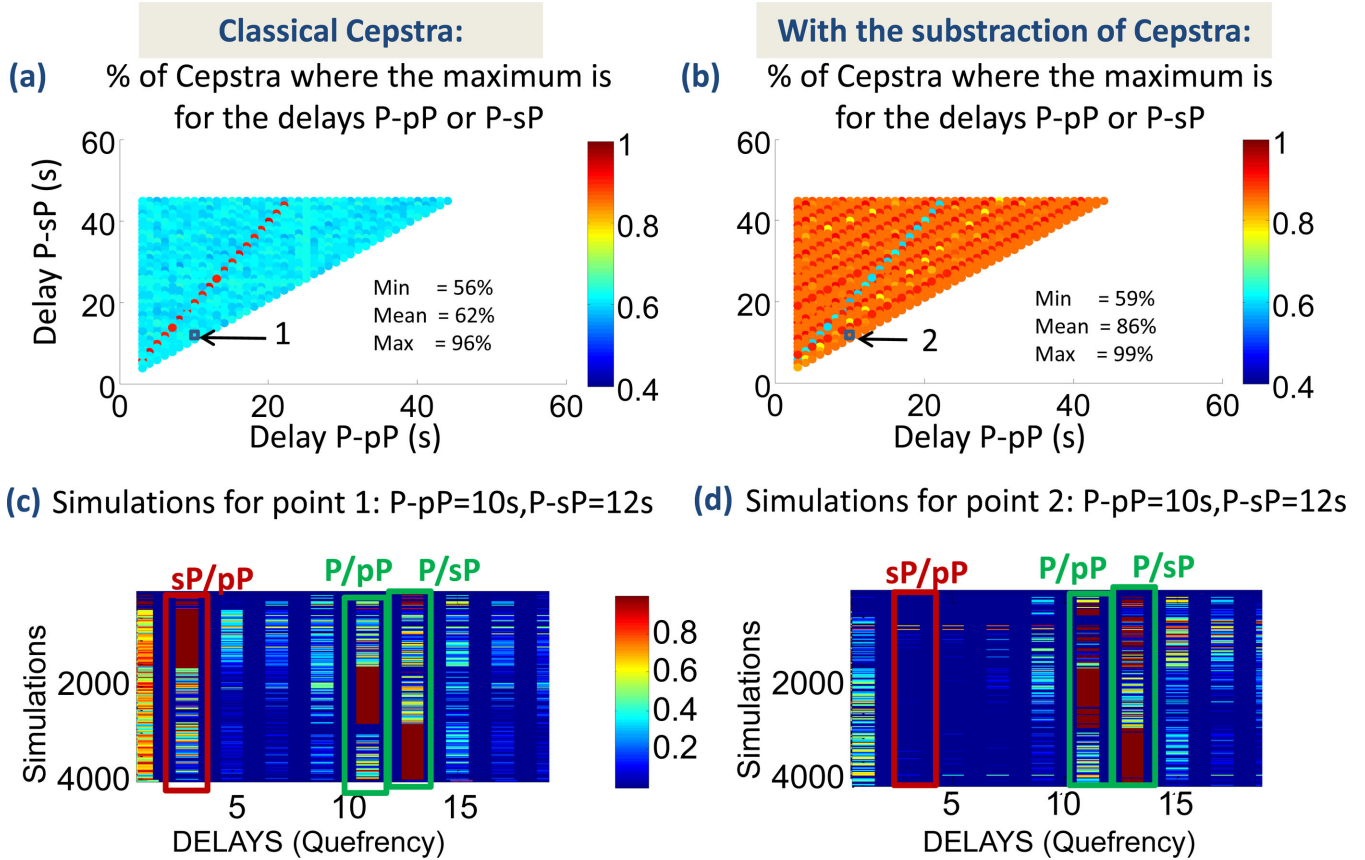
Figure 4. For different configurations of teleseismic signals with different P–pP and P–sP delays, representations of the percentages of the 4000 simulated cepstra (which are shown in (c) and (d) for a given configuration of the delays and with varying values of a_1, a_2, a_3) that have their main maximum for delays (P–sP) or (P–pP). (a) Using the classical cepstral analysis, the mean percentage of good detections of the depth phases is 62 per cent. Note that for P–pP = pP–sP, we reach 96 per cent. (b) Using the subtraction of the cepstra, the depth phases were successfully detected for 86 per cent of the simulations. Note that in the case where P–pP = pP–sP, the method is less adapted, at only 59 per cent. (c) Example of the simulated cepstra for the configuration with P–pP = 10 s and P–sP = 12 s, more than 25 per cent are sP–pP detections. (d) Example of the simulated cepstra for the configuration with P–pP = 10 s and P–sP = 12 s, where the incorrect sP–pP detections have been removed.

Table 1. The IASPEI91 GT5 events (with $M > 4.8$, from 2002).

Event	Latitude (°)	Longitude (°)	ISC depth (km)	ISC pP depth (km)	GT depth (km)	Cepstral depth (km)
GT1	16.8619	−100.01379	22	24	17.9	16.8
GT2	17.2099	−100.4780	29.6	32	25.4	32.2
GT3	16.9689	−100.2828	28	28	20.4	27.6

From eq. (15), the cepstral approach described above can be applied in the same way, to $S^n(t)$ instead of $S(t)$. The signal is normalized according to the maximum amplitude, then a_0, a_1, $a_2 < 1$.

Hence, using the convergence properties of the power functions for numbers below 1, there are three major improvements from using the power of the signal instead of the signal itself:

First, the amplitudes a_i^n will all be smaller than a_i, which makes the new values of $|X(w)|$ smaller than using the simple signal $f(t)$ (eq. 9). Thus, the assumption for the logarithm development becomes more adapted for small coefficients.

Secondly, the smallest amplitudes a_i^n will become even more negligible compared to the predominant amplitudes a_i^n (e.g. for $f(t)$ with $(a_1, a_2, a_3) = (0.9, 0.5, 0.1)$, the coefficients of $f'(t)^2$ are $(0.81, 0.25, 0.01)$: a_3 becomes negligible, and a_2 is more dominated by a_1). We then focus on the highest phase-arrival amplitudes, which are supposed to be the depth phases, as the effects of the free surface are assumed to give more energy to these depth phases than interface

reflected waves, which are supposed to reflect less energy, as a part is transmitted to the layer above. Hence, we decrease the effects of the small arrivals and tend to a case with only two predominant echoes, or even with only one echo, which are two configurations that we can deal with successfully.

The noise should be reduced (if the phases dominate the signal).

The advantage of this method is shown by a statistical test of the different configurations with different amplitudes and phases arrivals (Fig. 5). From the 86 per cent success using our new cepstrum method applied to the simple signal $f(t)$, we get around 90 per cent success for the same method and the same simulations, but applied to the signal $f(t)$ taken to the power of 2, 3 and 4. Finally, from the 62 per cent of the depth phase detections using the classical cepstrum approach, we can now obtain 90 per cent successful depth-phase detection. An example showing the great interest of using the power of the signal was extracted from a real signal from the Guerrero area, and can be seen in Fig. 6.
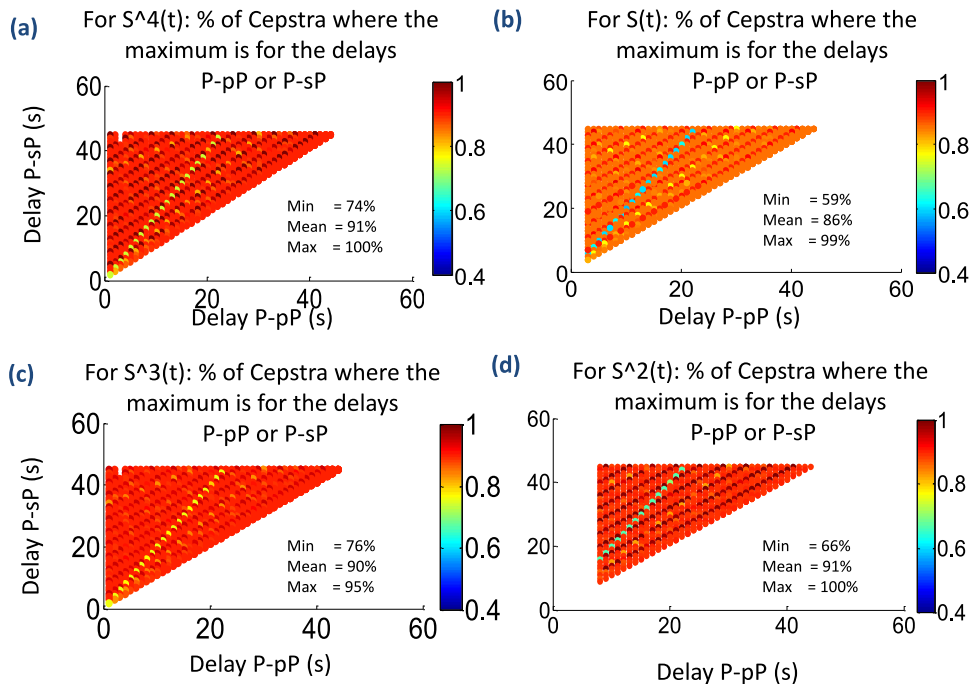
With the subtraction of Cepstra:

Figure 5. For different configurations of the teleseimic signal with different values for the delays P–pP and P–sP, representation of the percentage of the 4000 simulated cepstra (according to different values of a_1, a_2, a_3) that have their main maximum for the delays (P–sP) or (P–pP). (a) Using the subtraction method applied to the signal taken to the power of 4. (b) As (a), for the power of 1 (simple signal). (c) As (a), for the power of 3. (d) As (a), for the power of 2. The mean percentage of good detections of the depth phases is 90 per cent for (a), (c) and (d). For the power of 3 and 4 ((a), (c)), the configuration where P–pP = pP–sP reaches 75 per cent success, compared to the 59 per cent success for the simple signal (b).

Figure 6. (a) Recording of the GT2 event in the Guerrero area, at a depth of 25 km (Table 1), and where the localization is assumed to be well constrained. Three phases are detected: P, pP and sP. (b) Cepstrum analysis using eq. (5). Note that the different peaks in the cepstrum are related to different echoes in the signal. (c) Cepstrum analysis applied to the signal at a power 2 ($n = 2$ in eq. (9)). (d) as (c), for $n = 3$. (e) as (c), for $n = 4$. Only the major peak remains in the cepstral analysis.
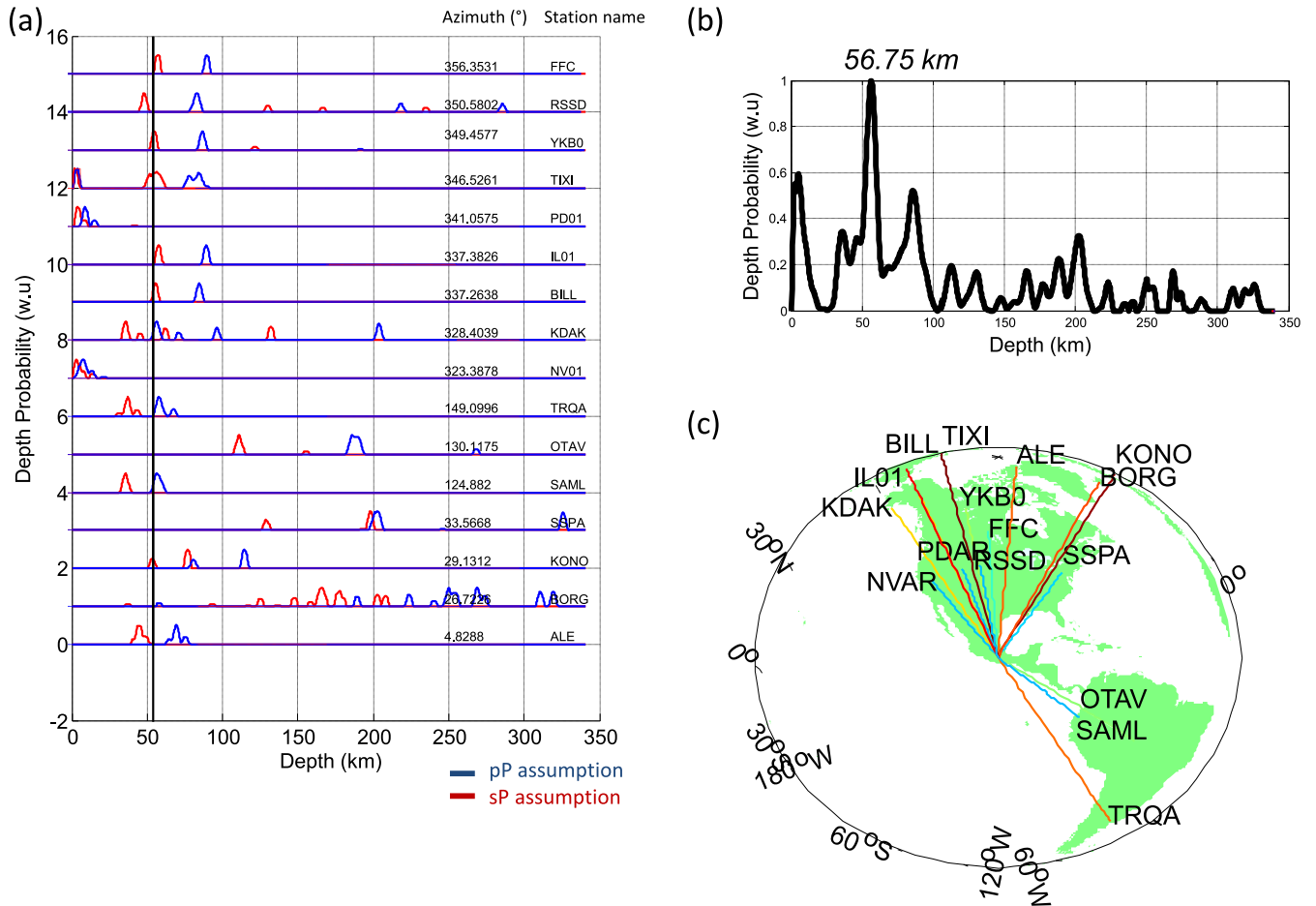
Figure 7. (a) Depth probability functions using the velocity IASPEI91model, as associated with P–pP delays (blue) and with P–sP delays (red). There is clear detection of sP in North America and pP in South America. (b) Final depth probability curve using the averages of the curves in (a). (c) Station distribution used for the automatic cepstral analysis.

Automatic analysis from the cepstral peaks to focal depth estimations

We first compute different cepstra for every recording of a station/array, where the seismic signals are taken respectively to the power of 1, 2, 3 and 4. We then apply the subtraction method for all of these estimated cepstra (as described above) to get a new set of improved cepstra. We finally apply the *F*-statistic procedure to this new set of cepstra, (following Letort *et al.* 2014), to give a final single depth probability curve (the *F*-statistic curve) associated to the array. This *F*-statistic curve for each station/array represents the probability of detection of the depth phases. As we are expecting pP or sP detections, we first assume these peaks to be P–pP delay detections, and the time delays are converted to a depth probability function using the velocity IASPEI91 model. Then, these time delays are associated to a P–sP delay, and another depth probability curve is obtained, which gives two different depth probability curves for each station/array. In Fig. 7(a), an example of these curves shows clear detection of sP in North America and pP in South America. These pairs of curves are finally simply summed in one single depth probability curve for each station, and a simple average procedure of these curves for the different azimuthal detections gives us our final depth solution, as shown in Fig. 7(b). For stability purposes, the proposed depth is then considered to be trustworthy if more than five different stations show a peak exactly for this final proposed depth.

Analysis of the cepstral method using synthetics

To validate the cepstral analysis, *P*-wave synthetic waveforms were built. For this, we used standard ray techniques, according to Bouchon (1976), Vallée *et al.* (2003) and Vallée (2004). Crust effects were taken into account by the reflectivity method of Fuchs & Müller (1971) and Mueller (1985), for both source and receiver. The mantle propagation was deduced from the IASPEI91 traveltime model (Kennett & Engdahl 1991), with a t^* of 0.6 s (Lundquist & Cormier 1980). The source duration was fixed at 1 s. Gaussian noise was added to the synthetic signal, such that the maximum of the signal was twice the level of the noise. This noise level definition can hide some of the phases completely in the noise. Fig. 8 shows an example of cepstral analysis for 15 stations with optimal azimuthal coverage and with a source depth of 30 km. The time window was selected as 80 s, and we filtered the synthetic recordings between 0.8 and 2.5 Hz (the same parameters are used for real recordings). The advantage of using the cepstral subtraction can be seen clearly: the source effect is well removed from the cepstrum and the main peak is directly linked to an echo of the direct *P* wave. The final result is 29 km, with a 1 km variation that is due the synthetic velocity model used.

In a second step, the synthetics were esimulated for an earthquake in the Guerrero area and for the 14 stations that were used in our inversion of real data (see Fig. 8). Random focal mechanisms for each depth were assumed, to study the relation between the mechanism
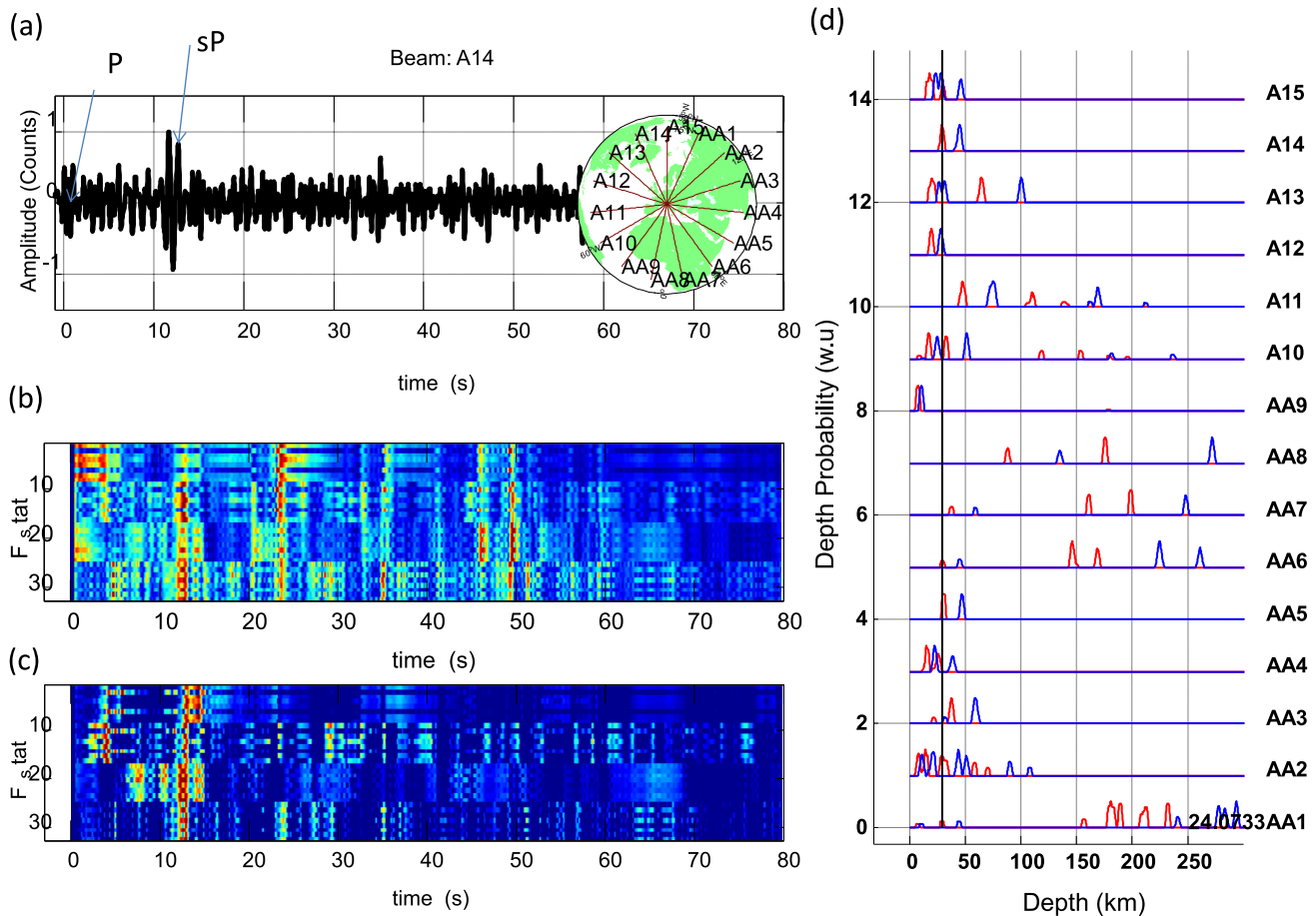
Figure 8. Synthetic example of an event at a depth of 30 km, and the cepstral analysis in the presence of Gaussian noise. (**a**) Synthetic signal for an event in Italy and a station in North America. The sP phase is the dominant phase in the signal, and the *P* wave is hidden in the noise. A map of the stations used is also shown. (**b**) Classical cepstral analysis (without the subtraction), with numerous echo detections noted. (**c**) New cepstral analysis (with subtraction), with the focus on the detection of the delay P–sP. (**d**) Final depth analysis, comparing all of the synthetic stations, with the final solution of 29 km.

and the station distribution, and to constrain the depth. Gaussian noise was added, to have a signal-to-noise ratio of 5.0. The source duration should be 1 s, and the moment magnitude was 5.0. Finally, two source crustals were investigated, as the standard crustal model from CRUST2.0, and the model modified with the introduction of a low velocity anomaly (5 km, with 5450 m s^{-1}) at 40 km, as Pérez-Campos *et al.* (2008) and Kim *et al.* (2010) showed that such a low velocity zone can be found in the Guerrero area, along the subduction interface. The key point of the method is to separate the direct *P* waves and the coda waves. Three fixed windows for the coda part were tested, one beginning from 12 s after the *P*-wave arrival, one from 7 s after, and one from 3 s after.

Generally this method is well adapted for any kind of focal mechanism and for any depth, except for a few outliers. That means that the results from our study in the Guerrero area should be trustworthy, as we used exactly the station distribution available for this area. Moreover, the cepstral subtraction methods (Figs 9b, d and e) allow more correct depth estimations to be found (each time, <20 earthquake depths only are incorrectly estimated) than for the classical cepstral analysis seen in Fig. 9a (with the empirical correction of the source term, following Letort *et al.* 2014, there were 36 events with incorrect depth estimations). The subtraction method is also improved by reducing the starting time for the second window (at 12 s, 7 s and 3s after the *P* wave; Figs 9b, d and e, respectively).

Some events for which the source is not well corrected (Figs 9a and b) give a final depth close to 0 (the cepstrum shows a peak for 0, related to the source). If the beginning time chosen for the assumed depth phases containing the window is longer than the real arrival time of the depth phases (Fig. 9b), this time window will contain little information about the source, and the subtraction method will not help to correct the source term. However, it will not degrade the solutions compared to the classic cepstral analysis (Fig. 9a). Using the optimal time to separate the *P* wave from the depth phases (Fig. 9e), there were no errors coming from the wrong correction of the source term. In the four analyses, we noted some events where major detection of pP phases without any coherent sP detection did not allow the two depth candidates to be dissociated (assuming pP or sP). The automatic conversion to equivalent depths gave incorrect depth estimations in these cases. We note also some bias in the depth estimation from 40 km. This comes from the IASPEI91 velocity model used, which would not be representative of the source velocities for deep events.

In practice, the whole direct *P* wave is assumed to arrive in the first 7 s after the theoretical arrival time. This time range is relatively large, as we did not use pickings, but instead, only the theoretical arrival time. However, it remains a good assumption in the Guerrero case and for the magnitude we are dealing with: the source duration should not exceed 2–3 s. Then, we applied the subtraction with one
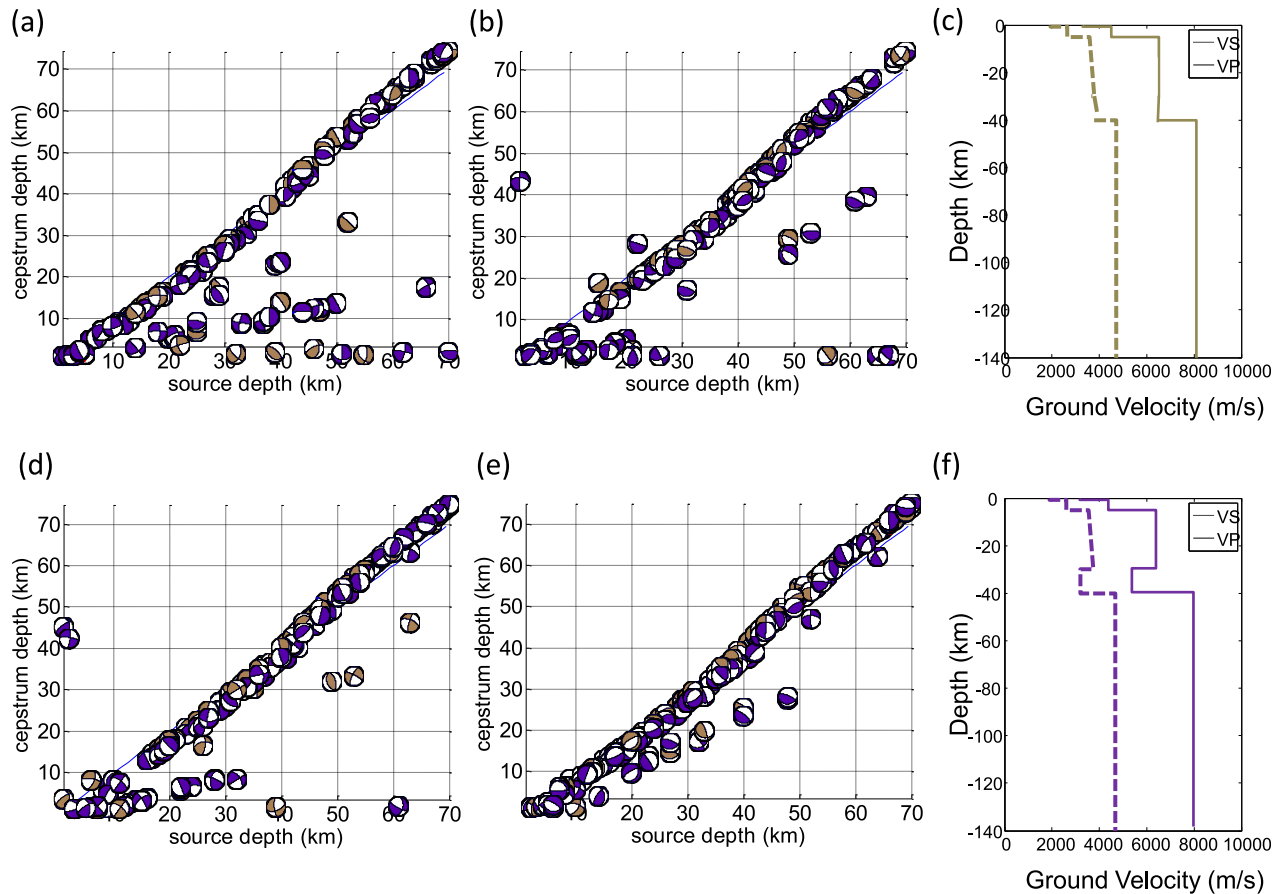
Figure 9. For the synthetic focal mechanisms built in the two-source velocity models shown in (c) and (f). (a) Estimated depths using the classical cepstrum analysis (with empirical correction of the source term, following Letort *et al.* 2014). The estimated depths with the new method using the subtraction of the cepstra of the coda part are shown in (b), (d) and (e). The different time windows were tested, to separate the coda part from the direct *P*-waves. (b) With the coda window beginning 12 s after the *P*-wave arrival. (d) Beginning 7 s after the *P*-wave arrival. (e) Beginning 3 s after the *P*-wave arrival.

window from 10 s before the theoretical *P* wave to 70 s after the *P* wave, and the second window with the assumed P-coda from 7 s after the *P* wave to 70 s after the *P* wave. Hence, the first window often contains the beginning of the P coda as well. In the specific case where the event is shallow (<10–15 km), with a weak direct *P*-wave and with predominant reflected phases in these first 7 s after the *P*-wave, the main peak in the cepstrum might be due to these phases and not to the *P*-wave, and might lead to the same errors in the depth estimation, as when using the old cepstral analysis. However, this exception is not frequent, and it can even be completely disregarded in our application to the Guerrero subduction, as we focused on the deeper parts of the subduction and with focal depths above a depth of 20 km.

Application to the Guerrero subduction area

The methodology described above was applied to the Guerrero subduction area. In all, 152 events in the ISC catalogue with magnitude >4.5 were selected. Using the epicenter localization given by the ISC catalogue, for each event and each station/array the theoretical *P*-wave arrival was first estimated automatically through the Ak135 tables. A large time window from 10 s before this theoretical *P*-wave arrival until 70 s after was specified, to ensure the selection of all of the useful direct *P* waves and coda *P* waves associated with each event (for the coda *P* waves, or P coda, these are the group of

different later phase arrivals that follow the direct *P* waves, and in particular the coda includes the pP, sP, PcP phases, and other possible reflections). Even in the case of mislocation and errors in the propagation tables, using this long time window includes all of the useful information. We then systematically filtered all of the spectra between 0.8 and 2.5 Hz, which is the frequency band of interest for earthquakes of magnitudes of around 4–5 in this area.

Fig. 10 illustrates the resulting inverted depths. From the 152 events, 101 were constrained successfully (more than five stations show coherent phase-arrival detection). Our new cepstral analysis better clusters event locations (Fig. 10c) compared to the ISC bulletin locations (Fig. 10a). Thus, it provides an improved view of the geometry of the subduction. In particular, the A-area in Figs 10 and 11 shows very stable depths of around 40–70 km, while the ISC catalogue varies between 50 and 100 km. This spacial coherency of the estimated cepstral depths is one of the first indications of the advantage of this method.

Moreover, we compared our results with the re-location of the same events using the new ISC-locator algorithm, following Bondár & Storchak (2011). This new location algorithm accounts for correlated error structure, and uses all of the IASPEI standard phases to obtain more accurate event locations. Bondár & Storchak (2011) demonstrated that through the use of later phases and testing for depth resolution, this new algorithm generally considerably clusters event locations more tightly compared to the ISC bulletin catalogue. The re-location of these 152 events from ISC-locator also
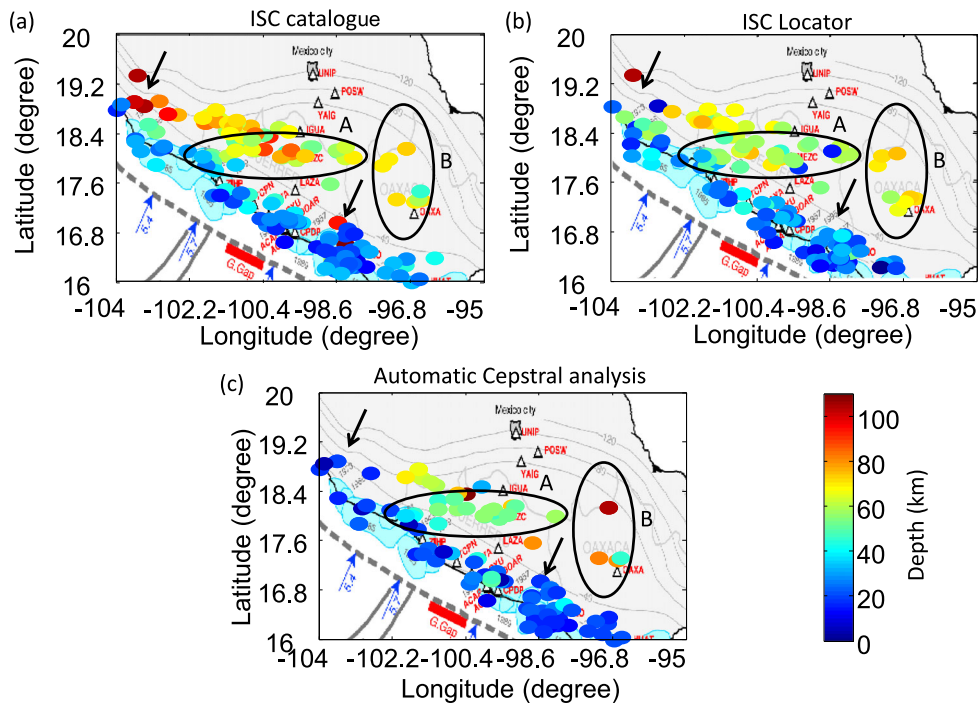
Figure 10. (a) Depths from the ISC catalogue. (b) Using the ISC-locator. (c) Using the cepstral analysis.

shows shallower events in the A area (Fig. 11a), which is consistent with our data. The focal depths obtained by the ISC-locator are closer to the cepstral analysis than to the ISC bulletin results (Figs 11b and c). However, even if the locations are close and consistent between these two methods, a bias of around 5–10 km still remains between the ISC-locator and the cepstral depths, as seen in Fig. 11(c).

The very deep earthquakes seen in the ISC catalogue (Fig. 10, arrows) are obviously due to errors in localization, as the two new methods (ISC-locator and cepstral analysis) do not confirm these

outliers. We have also checked the three ground thrust (GT5) events that were available for this area. These GT5 events are events for which the epicenter is known with an accuracy of <5 km (to a 95 per cent confidence level; Bondár & McLaughlin 2009). These three events are in good agreement with the cepstral analysis depths (Table 1, Fig. 11), and are closer to the ISC pP depth, another independent depth estimation from ISC that uses only depth phases (Bondár & Storchak 2011). These independent checks confirm the interest of our methodology and show that the estimated depths are reliable.
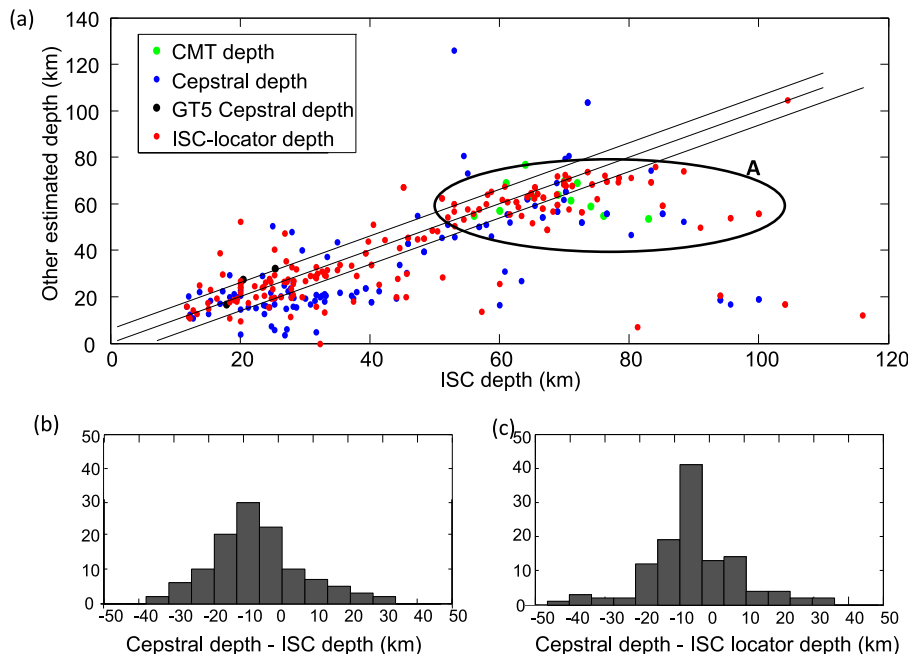

Figure 11. (a) ISC catalogue compared with the estimated depths using cepstral analysis, the ISC locator method, and the CMT (Table 2) and GT5 (Table 1) events catalogues. (b) Differences between the cepstral depths and the ISC catalogue depths. (c) Differences between the cepstral depths and the ISC-locator results.

Table 2. Common ISC/CMT events (with $M > 4.8$ and depth >40 km, from 2002).

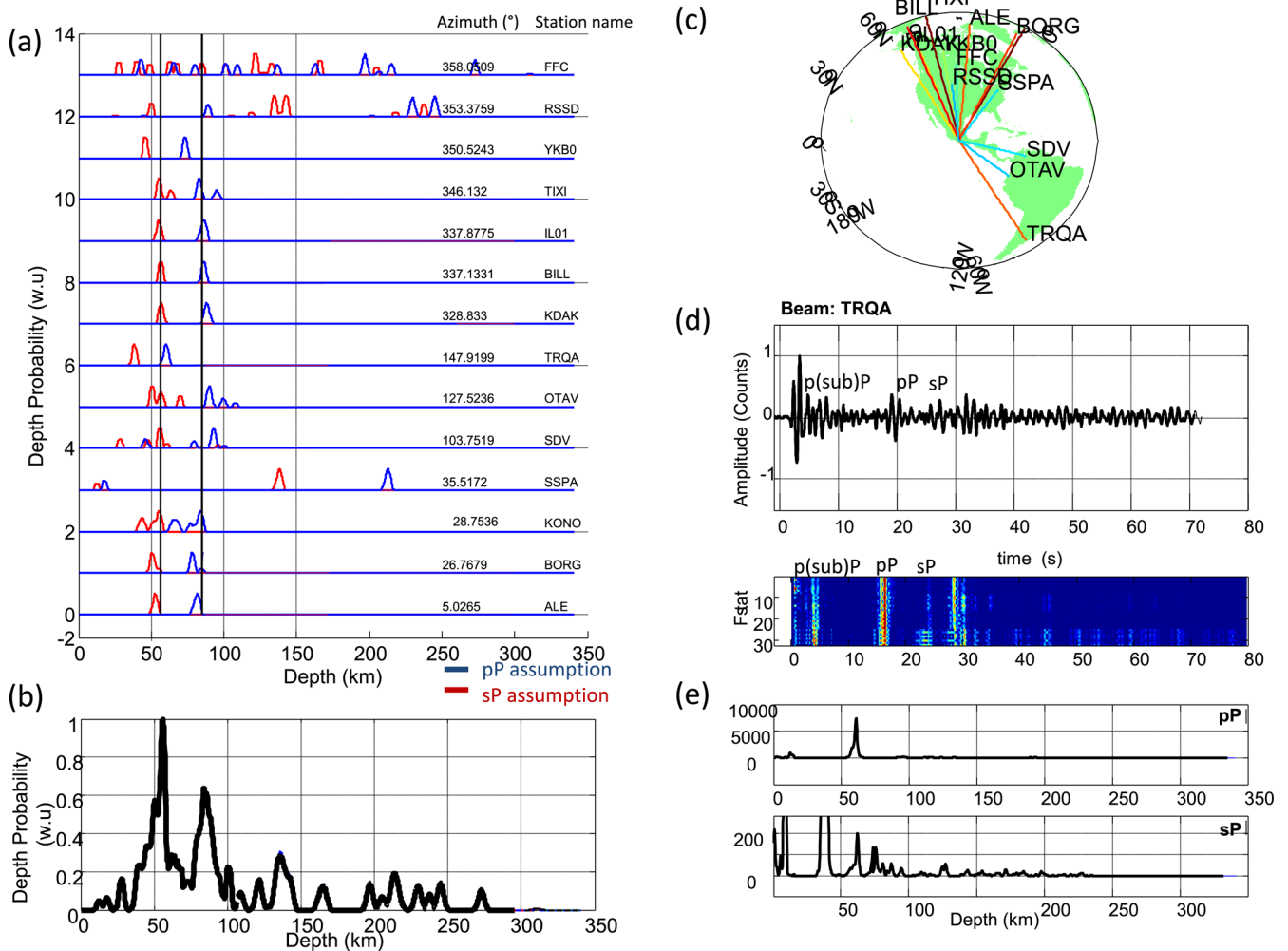| Event	Latitude (°)	Longitude (°)	ISC depth (km)	CMT depth (km)	MEX depth (km)	ISC pP depth (km)	Cepstral depth (km)
2003/05/16	18.29	−100.29	71	61.6	69	56	–
2003/07/21	18.5836	−101.0469	72	69	52	64	–
2005/12/14	18.4790	−101.1316	74	59	49	–	–
2006/02/20	18.2720	−100.6752	56	55	51	57	50.2
2006/03/20	18.6199	−101.8942	69	64	61	69	69
2006/08/11	18.5391	−101.0697	60	57	73	60	–
2007/07/28	18.3659	−100.600	83	53.5	57.6	83	74.5
2007/11/26	18.7572	−101.5563	70	70	54.4	70	65.2
2008/04/28	17.9941	−99.9706	76.5	55	57	76	56
2008/04/29	18.4920	−101.1359	65	63	49	65	59.2
2009/08/15	18.0998	−100.6157	61.2	69	57	61	55.5
2011/06/02	18.6156	−101.4834	64	77	20	64	62

Figure 12. (a) Depth probability functions using the velocity IASPEI91 model, which are associated with P–pP delays (blue) and P–sP delays (red). We show clear detection of sP and only one clear coherent pP detection for station TRQA. (b) Final depth probability curve using the averages of curves in (a). (c) Station distribution used for the automatic cepstral analysis. (d) Teleseismic signal recorded at station TRQA, which shows clear phase arrivals: the direct *P*-wave, the phase reflected on the surface of the subduction p(sub)P, the pP phase, and the sP phase. The cepstrum analysis shows three delays linked to the P phase (P–p(sub)P, P–pP P–sP) and one 'false' detection for a phase around 30 s, which is probably due to the later phase arrival in the P coda. (e) Final F-statistic curves assuming pP and sP detections. We note coherent P–pP and P–sP peaks for a focal depth of around 55 km, which validate the depth proposed in (b).

In our automatic cepstral analysis, the major part of the detected phases is sP phases, especially for the North America station (see Fig. 12). However, usually pP phases are more easily detected than sP phases. We hence checked the possibility of systematic error

in the automatic depth phase interpretation. For the example seen in Fig. 12(a), one station, TRQA, shows a clear pP phase when the others detect sP arrivals. A visual check of the TRQA signal shows a clear pP and a minor sP phase arrival (Fig. 12d) and the
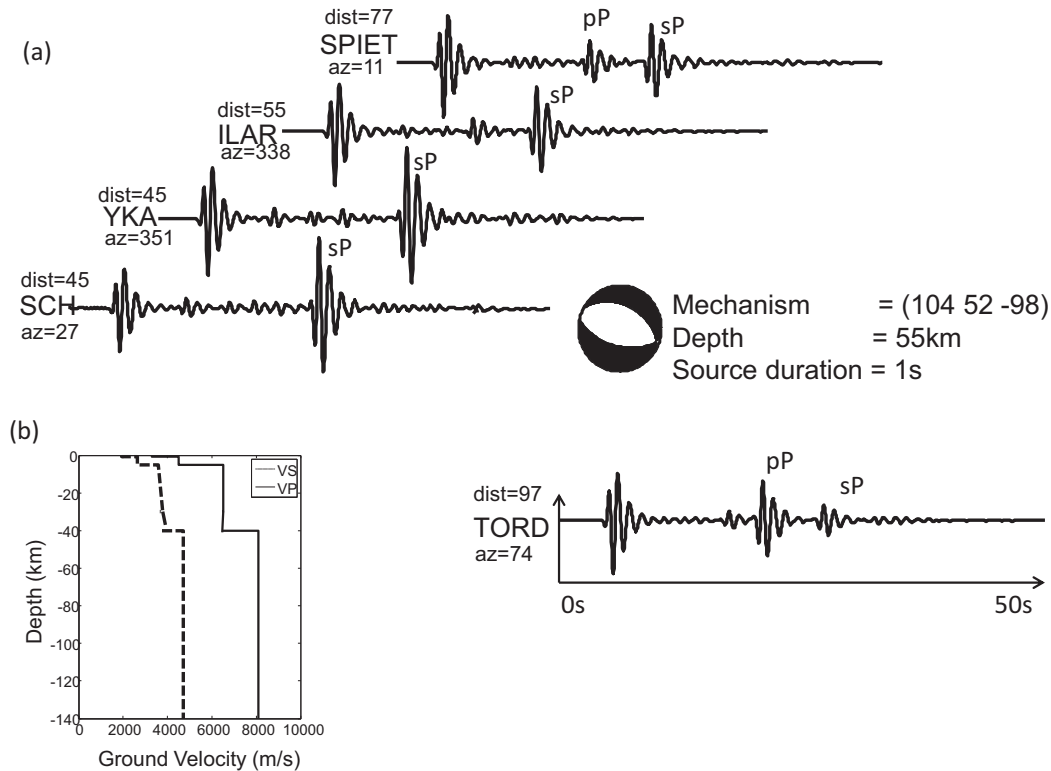
Figure 13. (a) Synthetic teleseismic recordings for a normal fault at 55 km in depth, which is typically the kind of mechanism expected for the Guerrero area. **(b)** The selected source velocity model. The predominant depth phases are the sP phases for North America. There are higher amplitudes for the sP phases than for the direct P phases for the two stations in Canada, SCH and YKA (Yellowknife array). For station TORD in Africa, a pP phase was detected.

cepstral analysis (Figs 12d and e) confirms these phase arrivals. These double coherent pP and sP arrivals in the same recordings are a good clue of the success of the depth estimation. Note also a possible interesting reflection on the surface of the subduction, marked as p(sub)P in Fig. 12(d).

To validate our important number of sP detections in North America, synthetic tests were conducted. According to the CMT solution and our knowledge of the area, the mechanisms are mainly thrust events. Computed synthetic recordings demonstrated that such events will show predominant sP detection in North America (Fig. 13). Once again, this is in full agreement with our results. Moreover, the bias between the estimated cepstral depths and ISC-locator depths can be explained by a misidentification of sP phases by pP phases (usually predominant and picked for analysis), which shows the great interest of using such an automatic cepstral analysis that is insensitive to the phase identification.

The new cepstral depths improve the knowledge of the Guerrero subduction geometry

The A-area (Fig. 11) is of great interest for understanding slow-slip silent earthquakes in this subduction zone. Indeed, the question of the origin of these slow-slip events is still debated, as coupling maps and slow-slip silent earthquake locations can show significant spatial variations on the subduction interfaces (Radiguet *et al.* 2012). Constraining the subduction geometry is thus crucial to understand the cause of these variations. The study of the Wadati-Benioff zone and hypocenter locations (Pardo & Suarez 1995) yields an idea of the subduction geometry, although it is limited by uncertainties in the depth estimation. Another method is to use receiver function

analysis (Pérez-Campos *et al.* 2008; Kim *et al.* 2010). A drawback of this approach is the scarce station coverage in the Guerrero region and a question about the lateral variation of the geometry that remains open. Our cepstral analysis is thus a powerful tool to obtain images of the subduction geometry. We clearly see a flat area on both sides of the receiver line, where the slow-slip silent earthquakes occur (Fig. 11).

To confirm our results and as the ISC-locator data are interesting, we used this new algorithm to re-locate all of the seismicity in the Guerrero area since 1964 (19 993 events), from the ISC catalogue depths. We assumed that the major part of the seismicity was due to the plate interface or located at the subducted plate. We then removed from the catalogue the shallow earthquakes that were obviously not related to the plate interface in the deeper part of the subduction (from 100 km to the coast; the subduction is around a depth of 40 km, and so all of the earthquakes far from the coast and with focal depth below 20 km were discarded). We then empirically defined an average moving window with a radius of 0.25°, computed the average depth of this window if more than 50 focal depths are included in this radius, and investigated in this way the whole subduction area through a grid of 0.05° × 0.05° (Fig. 14).

In this way, assuming the seismicity is intraplate seismicity, we drew up an improved view of the seismicity in this area (Fig. 14). As noted by the cepstral depth analysis, we can still note the lack of lateral geometry variations in the deeper parts of the subduction, where the slow-slip occurs. In Fig. 14, we also superimposed our cepstral depths on this averaged seismicity from ISC-locator, which showed great similarities. One interesting observation is that we did not notice here any significant bias between cepstral depths and the ISC-locator averaged depths. Our interpretation is that the whole relocated seismicity is mainly due to small events (magnitude around 3).
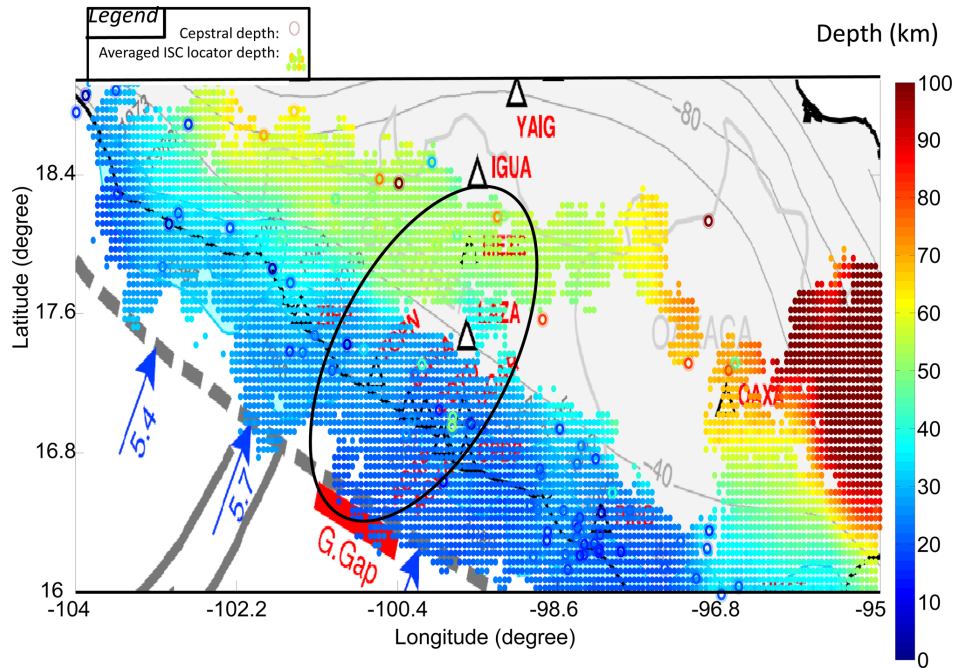
Figure 14. Final cepstral depth (circles) for the Guerrero area. The averaged seismicity was superimposed from the ISC-locator locations (dots): for an average moving window with a radius of 0.25°, the average depth in this window was computed, through a grid of 0.05° × 0.05°. The slow-slip events are inside the ellipse, by the Guerrero gap (red).

These small magnitude events show no depth phases and have important punctual uncertainties, although they are, on average, a good representation of the mean seismicity, due to the important amount of data. For the high magnitude earthquakes (>4.5), the uncertainties are less important, as depth phases are detected in the catalogues, although some systematic errors appear because of the misinterpretation of these phases (e.g. pP, instead of sP). For these high magnitudes, the cepstral analysis manages to correctly constrain the depth, coherent with the mean seismicity.

CONCLUSION

We have developed a new, blind and automatic depth-estimation method that is based on cepstral analysis. This new method has been applied to 152 events in the Guerrero subduction area (Mexico). Our new cepstral analysis better clusters the event locations compared to the ISC bulletin. The spatial coherency of the estimated cepstral depths and the relocation of the same events using the ISC-locator algorithm (Bondár & Storchak 2011) show the efficiency of our completely automatic method. Both methods show good agreement in most cases, and both indicate overestimation of focal depths in the classical ISC catalogue for the deeper part of the subduction.

The main limitation of our method is the use of a global velocity model (IASPEI91), which might not be a good local representation of the source-area wave velocities. However, the results of this method are particularly sensitive to the relative depth variations between events, and the relative lateral variations in the seismicity appear to be well constrained. The method also has the great advantage of being robust in the presence of noise: a signal-to-noise of around 2.0 in the synthetic data is enough to estimate the depth in good azimuthal coverage configuration. The use of synthetic examples also demonstrates that the method is well adapted to estimate the depths of a group of events. However, the method cannot evaluate the depths of earthquakes for rare configurations, where the station distribution, the mechanisms, and the source ve-

locities produce only pP or only sP phases. A solution is to interpret these cases assuming pP detection, as it is commonly admitted that it is more common to see pP than sP phases. Hence, any punctual depth estimation in a non-optimal azimuthal configuration should then be taken with care. For suboceanic events, the depth estimation may also be biased by a misinterpretation of phases reflected in the surface of the sea (pwP) by phases reflected on the surface of the crust (pP). This misinterpretation can lead to depth estimation errors of more than 10 km. Note also that for shorter station distances (<29°), we can sometimes noted different phase arrivals in the teleseismic recordings. For distance ranges around 28°, a pair of well-dissociated direct *P*-wave arrivals can be observed (and pairs of pP, sP phases as well), coming from the propagation of the *P* wave below or above the upper/lower mantle boundary. Interpreting the observed phases for these short distances might thus be challenging.

For applications of sets of events (e.g. aftershocks, subduction area), the automatic cepstral analysis appears to be a powerful tool to better constrain the geometry of the area of interest. This new method should now be applied in a more systematic way, to improve the focal depths of moderate earthquakes in other tectonic contexts, and it could provide improved global catalogues for moderate intraplate and interplate seismicity.

REFERENCES

Bondár, I. & McLaughlin, K., 2009. A new ground truth data set for seismic studies, *Seism. Res. Lett.,* **80,** 465–472.

Bondár, I. & Storchak, D., 2011. Improved location procedures at the International Seismological Centre, *Geophys. J. Int.,* **186,** 1220–1244.

Bondár, I., Myers, S.C., Engdahl, E.R. & Bergman, E.A., 2004. Epicenter accuracy based on seismic network criteria, *Geophys. J. Int.,* **156,** 483–496.

Bonner, J., Reiter, D. & Shumway, R., 2002. Application of a cepstral Fstatistic for improved depth estimation, *Bull. seism. Soc. Am.,* **92,** 1675–1693.

Bouchon, M., 1976. Teleseismic body wave radiation from a seismic source in a layered medium, *Geophys. J. R. astr. Soc.,* **47,** 515–530.

Childers, D.G., Skinner, D.P. & Kemerait, R.C., 1977. The cepstrum: a guide to processing, in *Proceedings of the IEEE 65,* no. 10, pp. 1428–1443.

Cohen, T.J., 1970. Source-depth determinations using spectral, pseudoautocorrelationand cepstral analysis, *Geophys. J. R. astr. Soc.,* **20,** 223–231.

Engdahl, E.R., van der Hilst, R. & Buland, R., 1998. Global teleseismicearthquake relocation with improved travel times and procedures for depth determination, *Bull. seism. Soc. Am.,* **88,** 722–743.

Fuchs, K. & Müller, G., 1971. Computation of synthetic seismograms with the reflectivity method and comparison with observations, *Geophys. J. R. astr. Soc.,* **23,** 417–433.

Kennett, B.L.N. & Engdahl, E.R., 1991. Travel times for global earthquake location and phase association, *Geophys. J. Int.,* **105,** 429–465.

Kim, Y., Clayton, R.W. & Jackson, J.M., 2010. Geometry and seismic properties of the subducting Cocos plate in central Mexico, *J. geophys. Res.,* **115,** B06310, doi:10.1029/2009JB006942.

Letort, J., Vergoz, J., Guilbert, J., Cotton, F., Sebe, O. & Cano, Y., 2014. Moderate earthquake teleseismic depth estimations: new methods and use of the comprehensive nuclear-test-ban treaty organization network data, *Bull. seism. Soc. Am.,* **104**(2), doi:10.1785/0120130126.

Lundquist, G. & Cormier, V., 1980. Constraints on the absorption band model of Q, *J. geophys. Res.,* **85,** 5244–5256.

Mueller, C.S., 1985. Source pulse enhancement by deconvolution of an empirical Green's function, *Geophys. Res. Lett.,* **12,** 33–36.

Pardo, M. & Suarez, G., 1995. Shape of the subductedrivera and cocos plates in southern mexico: seismic and tectonic implications, *J. geophys. Res.,* **100**(B7), 12 357–12 373.

Pearce, R.G. & Rogers, R.M., 1989. Determination of earthquake moment tensors from teleseismic relative amplitude observations, *J. geophys. Res.,* **94**(B1), 775–786.

Pérez-Campos, X. *et al.*, 2008. Horizontal subduction and truncation of the Cocos plate beneath central mexico, *Geophys. Res. Lett.,* **35,** L18303, doi:10.1029/2008GL035127.

Radiguet, M., Cotton, F., Vergnolle, M., Campillo, M., Walpersdorf, A., Cotte, N. & Kostoglodo, V., 2012. Slow slip events and strain accumulation in the Guerrero gap, Mexico, *J. geophys. Res.,* **117**(B4), doi:10.1029/2011JB008801.

Vallée, M., 2004. Stabilizing the empirical Green function analysis: development of the projected Landweber method, *Bull. seism. Soc. Am.,* **94,** 394–409.

Vallée, M., Bouchon, M. & Schwartz, S.Y., 2003. The 13 January 2001 El Salvador earthquake: a multidata analysis, *J. geophys. Res.,* **108,** 2203–2208.